
GENERAL FORMULATION OF AN ANALYTIC AND LIPSCHITZ CONTINUOUS CONTROL ALLOCATION FOR THRUST-VECTORED CONTROLLED RIGID-BODIES*

Frank Mukwege

SAAS – Control and System Analysis Department
Université Libre de Bruxelles (ULB)
Avenue Franklin Roosevelt 50, CP 165/55, Brussels, Belgium
frank.mukwege@ulb.be

Tam Willy Nguyen

Department of Electrical Engineering
Kyoto University
615-8510 Kyoto, Japan
nguyen.tamwilly.3e@kyoto-u.ac.jp

Emanuele Garone

SAAS – Control and System Analysis Department
Université Libre de Bruxelles (ULB)
Avenue Franklin Roosevelt 50, CP 165/55, Brussels, Belgium
emanuele.garone@ulb.be

October 10, 2025

ABSTRACT

This paper¹ presents a general framework for the control allocation problem (CAP) in thrust-vector controlled rigid-bodies. This study introduces a systematic and scalable method for arbitrary rigid-bodies equipped with vectorized thrusters. Two novel solutions are proposed: a closed-form, Lipschitz continuous mapping that ensures smooth actuator orientation references, and a convex optimization formulation capable of handling practical actuator constraints such as thrust saturation and angular rate limits. Both methods leverage the null-space structure of the allocation mapping to perform singularity avoidance while generating sub-optimal yet practical solutions. The effectiveness and generality of the proposed framework are demonstrated through numerical simulations on a 3DOF marine vessel and a 6DOF aerial quadcopter.

1 Introduction

Control allocation problems manifest when there exists an excess of control signals in comparison to the commanded forces and moments, making the system fully- or overactuated. Control allocation techniques are employed to efficiently harness this redundancy of actuators in order to collectively generate the total forces and moments commanded by a higher-level controller. Moreover, control allocation aims to optimize power consumption, accommodate actuator constraints, and address other specified objectives or constraints. Control allocation is a common problem in various fields such as aerospace, aeronautics, marine systems and others vehicles ([1]).

In this work, we will present a general framework for control allocation of overactuated rigid bodies equipped with vectorized thrusters, i.e propulsion units capable of producing a thrust T in a given direction. Thrust vectoring is particularly useful to enable overactuation in systems while using less physical actuators on board. Indeed, one can mention 3D nozzles used in military aircrafts and rockets, 2D azimuth thrusters (electric or gasoline pods) of marine vessels (Figure 1) or 2D tiltable propellers of multi-rotor UAVs. Solving the control allocation is finding the control

¹This is the authors' original version of a manuscript submitted to *Automatica* (Elsevier). The content may differ from the final published version. Distributed under the arXiv non-exclusive license to distribute.

signals to send to the actuators in order to produce the requested sets of generalized forces and torques τ_d . In the early 90s, most of the solutions for the control allocation problem (CAP) originated from the aeronautics community. These were mostly closed-form solution based on the Moore-Penrose pseudo-inverse and the exploitation of the null-space ([2, 3, 4, 5]). While those closed-form and other solutions were fast and easy to implement, they were sensible to the singularities. A singularity is an actuator configuration where the set of actuators is unable to produce the generalized forces in all directions without first changing their orientations. Since the effectors usually have a finite turning rate, crossing these singularities induces a period of time where the system is not able to fulfill the demands of the high-level controller or to respond to any fast environmental forces. Although these singularities are problematic, they are also usually related to energy-efficient configurations. Therefore, handling these singularities involves a tradeoff between optimality in terms of energy consumption and stability of the closed-loop system.

To address the various challenges of the CAP, within the marine community the predominant direction taken involves solving the CAP through online optimization methods. In [6], the authors introduce a control-Lyapunov design paradigm to tackle the CAP employing nonlinear optimization techniques. The seminal work by [7] presents a sequential quadratic programming strategy. The fundamental concept of this paper revolves around addressing a quadratic program at each time step, providing a local approximation of a nonlinear CAP. To handle singularities, a penalty term is incorporated into the cost function, effective solely against linearly dependent configurations and only possible when dealing with 3 or more actuators. In [8], the authors propose a convex quadratic representation of the CAP, accounting for saturation and angular linear constraints but omitting a singularity avoidance mechanism. This solution is based off Sordalen's [9] extended representation. A novel constrained control allocation method is detailed in [10], emphasizing a predictive methodology to compute the subsequent set of actuator inputs at each sample. Tailored to the case of the CAP under slow and predictable weather disturbances, the performance of the solution drops and can be sensible to singular configurations in the case of unpredictable and extreme weather. The work by [11] introduces a Cartesian thrust allocation approach, addressing CAP for 3DOF marine vessels with a diverse range of actuators, including tunnel thrusters or variable direction thrusters. Although constraints such as turn rate limits and thrust saturation are considered, the singularity avoidance solution proposed is only applicable for systems with more than 2 actuators. In [12], an algorithm for control allocation in double-ended ferries with azimuth thrusters is presented. This method reformulates the problem as a scalar-bounded optimization problem, facilitating efficient online resolution. Nonetheless, it also lacks a singularity avoidance mechanism. In [13], a novel constrained control allocation method for ships with azimuth thrusters using deep neural networks is proposed for a dynamic positioning context. This approach has been also investigated within the aerospace community as [14, 15] applied this solution to respectively a near-space vehicle and a space re-entry vehicle. Finally, in [16], following approaches from the aerospace community of the 90s, the authors propose an optimal predictive control scheme for managing a quadcopter's manipulation of a ground-anchored object. The controller handling both the allocation and the stabilisation, ingeniously leverages the quadcopter's attitude nullspace to compute the optimal sequence of controls and attitude references.

This paper introduces two solutions for the control allocation problem tailored specifically for thrust-vector controlled rigid-bodies. The first solution is a Lipschitz continuous closed-form method, offering robust stability guarantees. The second solution is optimization-based, reshaping the problem into a convex form, and capable of effectively managing common actuator constraints such as thrust rate, saturation and angular rate. These 2 results will be illustrated by numerical examples on a 2D surface vessel with azimuth thrusters and on a 3D aerial quadcopter with tilting rotors.

2 Problem Description

Let us consider a rigid-body with n degrees of freedom (DOF) and m vectorized actuators and let us also consider a body frame \mathbf{B} associated to it. For each i^{th} actuator we also define the reference frame \mathbf{A}_i , centered in the actuator and its z -axis points in the direction of the produced thrust T (See Figure 1). The forces and torques produced by this actuator in the frame \mathbf{A}_i are

$$\mathbf{f}_{\mathbf{A}_i} = \begin{bmatrix} 0 \\ 0 \\ 1 \end{bmatrix} T_i, \quad \boldsymbol{\tau}_{\mathbf{A}_i} = \begin{bmatrix} 0 \\ 0 \\ -s_i \kappa_{d_i} \end{bmatrix} T_i, \quad (1)$$

where T_i is the thrust produced by the i^{th} actuator. In the case of propellers $\kappa_d \in \mathbb{R}_0^+$ is a proportional factor between the thrust and reaction torque depending on the application (e.g. for helicopters, κ_{d_i} is the length of the propeller blade), $s_i = \pm 1$ represents the spin direction which implies the orientation of the reaction torque produced by the rotation of the propeller. For other type of thrusters (e.g. nozzles) which do not produce reaction torque, $\kappa_{d_i}, s_i = 0$. Note that in this work, we assume unidirectional thrusters and therefore assume $T_i \geq 0$.

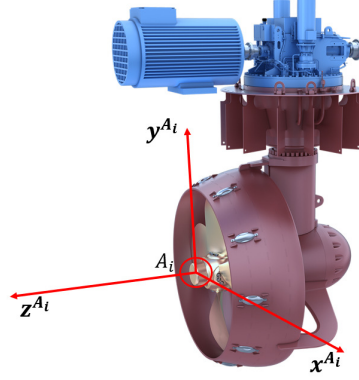


Figure 1: Example of an actuator frame for an azimuth thruster from [17]

The forces and torques produced by the i^{th} actuator in the body frame B are

$$\tau_{d_i} = \begin{bmatrix} R_{A_i}^B & 0_{3 \times 3} \\ S(p_{A_i}^B) R_{A_i}^B & R_{A_i}^B \end{bmatrix} \begin{bmatrix} 0 \\ 0 \\ 1 \\ 0 \\ 0 \\ -s_i \kappa_{d_i} \end{bmatrix} T_i \quad (2)$$

where $R_{A_i}^B$ is the SO(3) rotation matrix from A_i to B , where $p_{A_i}^B$ is the position of A_i in the reference frame B and $S(p_{A_i}^B)$ the skew-symmetric matrix equivalent to the cross product between a vector. With $p_{A_i}^B = [p_x, p_y, p_z]$,

$$S(p_{A_i}^B) = \begin{bmatrix} 0 & -p_z & p_y \\ p_z & 0 & -p_x \\ -p_y & p_x & 0 \end{bmatrix}. \quad (3)$$

Through some manipulation of (2), it is possible to rewrite τ_{d_i} in the compact form

$$\tau_{d_i} = M_i \hat{v}_i T_i \quad (4)$$

where $M_i \in \mathbb{R}^{6 \times 3}$ is defined as

$$M_i = \begin{bmatrix} I_{3 \times 3} \\ S(p_{A_i}^B) - s_i \kappa_{d_i} I_{3 \times 3} \end{bmatrix}, \quad (5)$$

$\hat{v}_i \in S^2$ is a unit vector defined as the third column of the rotation matrix $R_{A_i}^B$ and represents the direction towards which the actuator is pointed. At this point, by summing all torque vectors, it is possible to get the effect of all the actuators on the rigid body as

$$\tau = \sum_{i=1}^m M_i \hat{v}_i T_i \quad (6)$$

$$= M \operatorname{diag}_3 \left(\begin{bmatrix} \hat{v}_1 \\ \dots \\ \hat{v}_m \end{bmatrix} \right) \begin{bmatrix} T_1 \\ \dots \\ T_m \end{bmatrix}, \quad (7)$$

where $\tau = [F_x, F_y, F_z, \tau_x, \tau_y, \tau_z]^T$, the matrix M is

$$M = \begin{bmatrix} I_{3 \times 3} & \dots & I_{3 \times 3} \\ S(p_{A_1}^B) - s_1 \kappa_{d_1} I_{3 \times 3} & \dots & S(p_{A_m}^B) - s_m \kappa_{d_m} I_{3 \times 3} \end{bmatrix},$$

and $\operatorname{diag}_3 : \mathbb{R}^{3m \times 1} \rightarrow \mathbb{R}^{3m \times m}$ is a matrix operator defined as

$$\operatorname{diag}_3 \left(\begin{bmatrix} \hat{v}_1 \\ \dots \\ \hat{v}_m \end{bmatrix} \right) = \begin{bmatrix} \hat{v}_1 & 0_{3 \times 1} & \dots & 0_{3 \times 1} \\ 0_{3 \times 1} & \hat{v}_2 & \dots & 0_{3 \times 1} \\ 0_{3 \times 1} & 0_{3 \times 1} & \dots & \hat{v}_m \end{bmatrix}.$$

Unlike in the case of fixed actuators, in this paper we consider vectorized actuator where it is possible to vary not only

the thrust T_i but also the orientation of the actuator $\hat{v}_i \in S^2$. The orientation of the actuators is governed by servos that can move it around two axes of rotation : the azimuth $\beta_i \in [-\pi, \pi]$ and the elevation $\alpha_i \in [-\pi, \pi]$. Accordingly each vector \hat{v}_i can be parameterized as

$$\hat{v}_i(\alpha_i, \beta_i) = \begin{bmatrix} \sin(\alpha_i)\cos(\beta_i) \\ \sin(\alpha_i)\sin(\beta_i) \\ \cos(\alpha_i) \end{bmatrix}. \quad (8)$$

At this point it is possible to rewrite (6) as

$$\tau = M \text{diag}_3 \left(\begin{bmatrix} \hat{v}_1(\alpha_1, \beta_1) \\ \vdots \\ \hat{v}_m(\alpha_m, \beta_m) \end{bmatrix} \right) \begin{bmatrix} T_1 \\ \vdots \\ T_m \end{bmatrix} \quad (9)$$

$$= J(\theta)T, \quad (10)$$

where $\theta = [\alpha_1, \beta_1, \dots, \alpha_m, \beta_m]^T$, $T = [T_1, \dots, T_m]^T$ and the matrix $J(\theta)$ is defined as

$$J(\theta) = M \text{diag}_3 \left(\begin{bmatrix} \hat{v}_1(\alpha_1, \beta_1) \\ \dots \\ \hat{v}_m(\alpha_m, \beta_m) \end{bmatrix} \right). \quad (11)$$

In this setting, the Control Allocation Problem (CAP) can be defined as follows:

Control Allocation Problem (CAP) - Given a desired generalized torque τ_d , find actuators orientations $\bar{\theta}$ and thrusts \bar{T} such that $\tau_d = J(\bar{\theta})\bar{T}$.

Many variants of these problems can be formulated depending on possible different cost functions, constraints on the input as presented in [7]. One of the basic variants is to choose, among the possible solutions, the one that minimizes some norm of the thrust while T and θ are possibly subject to constraints. The basic case is the case where one wants to minimize a quadratic cost of the thrust subject to positivity constraints of the thrust. In this case it is convenient to rewrite (2) in the so-called *extended representation* ([9]). The main idea is to rewrite (10) as

$$\tau = MF, \quad (12)$$

where $F = [F_1 F_2 \dots F_m]^T$ and $F_i = \hat{v}_i(\alpha_i, \beta_i)T_i$. Doing so, the solution that minimizes the square of F^* is obtained using the Moore-Penrose pseudo-inverse of M

$$F^* = M^\dagger \tau_d. \quad (13)$$

Once the vector F^* is obtained, the optimal thrust T_i^* and orientations of each thrusters α_i^*, β_i^* are

$$T_i^* = \|F_i^*\|, \quad (14)$$

$$\beta_i^* = \text{atan2}(F_{y_i}, F_{x_i}), \quad (15)$$

$$\alpha_i^* = \text{atan2}\left(F_{z_i}, \sqrt{F_{y_i}^2 + F_{x_i}^2}\right). \quad (16)$$

Remark 1 - Interestingly enough, even in the case F is subject to linear equality constraints in the form $AF = b$, the optimal solution of this problem can be computed in closed form as

$$F^* = \begin{bmatrix} M \\ A \end{bmatrix}^\dagger \begin{bmatrix} \tau_d \\ b \end{bmatrix}. \quad (17)$$

This result is particularly useful in the case some actuators can be oriented only in one degree of freedom. For instance if only the elevation α_i can be modified and the azimuth is $\beta_i = 0$, this translates into the constraint $[0 \ 1 \ 0] F_i = 0$. \square

Remark 2 - In some cases we might be interested in controlling the generation of forces and torques only along certain direction and the effect in others is not of interest. To tackle this case we introduce the matrix $P \in \mathbb{R}^{6 \times l}$ as a basis for the subspace in which we are interested to generate our torques/forces. For instance in the case of a vessel for which we are interested in generating forces and torques only on the x-y plane, $l = 3$ and P is

$$P = [e_1 \ e_2 \ e_6]. \quad (18)$$

where $e_i \in \mathbb{R}^6$ is the i^{th} vector of the canonical basis. The matrix P can be then used to “cancel” the lines of (12) we are not interested obtaining $P^T \tau = P^T M F$. Accordingly, in this case, the optimal solution of the CAP is

$$F^* = (P^T M)^\dagger P^T \tau. \quad (19)$$

□

The main drawback of the pseudo-inverse approach is that, although very easy to compute and to implement, it presents discontinuities in the orientations θ . Since these angles are governed by servos that cannot instantaneously jump from one position to another, this is a major problem which can potentially lead to undesired behaviors such as reduced bandwidth of the actuation and consequent undesired oscillations.

The conventional approach in the marine literature to address this problem is to rewrite the CAP as a nonconvex optimization problem to be solved at discrete time intervals (see e.g., [7, 18, 19, 12, 20]).

In our early paper ([21]) we proposed a solution to this angular discontinuity problems for the specific case of a 3DOF vessel with two azimuth thrusters. Such solution drastically departs from the existing literature as it provides a systematic methodology to build sub-optimal closed-form mappings that are Lipschitz continuous. We also showed that, with some manipulation, the same results can be used to better deal with all types of singularities compared with what exists in the literature, and that moreover this can be done using convex optimization.

In this paper we will present a nontrivial extension of our early result to the general case of a 6DOF rigid body and an arbitrary number of actuators.

In particular the following sections we will :

- propose a systematic approach to build closed-form, sub-optimal Lipschitz continuous solutions of the CAP for thrust-vector controlled rigid bodies which allow to trade-off between continuity and optimality while addressing all types of singularities;
- propose a convex formulation of the CAP (36)-(37) for a wide class of rigid-bodies with actuators constraints such as thrust saturation and angular rate. This will be done by exploiting the closed-form solution to construct a new cost function.

3 Lipschitz continuous solution of the CAP in closed-form

The starting point of our analysis is the observation that all the solutions $F \in \mathbb{R}^{3m \times 1}$ to equation (10) can be written as the optimal solution F^* plus a vector in the null-space of the matrix M , i.e.

$$F = M^\dagger \tau_d + z, \quad (20)$$

where $z \in \text{Ker}\{M\}$ and $M^\dagger \in \mathbb{R}^{3m \times 6}$. The main idea of the proposed solution is to use the vectors of the null space to “smooth” the optimal mapping (13). In particular the idea is to build a suboptimal mapping in the form

$$F = F^* + s(\tau_d), \quad (21)$$

where $F^* = M^\dagger \tau_d$ and $s(\tau_d) = [s_1^T(\tau_d), \dots, s_m^T(\tau_d)]^T$ is a function $s(\cdot) : \mathbb{R}^6 \rightarrow \text{Ker}\{M\}$ that generates a smoothing vector designed to ensure the continuity of the vector θ . This condition translates the continuity of \hat{F} vector of the orientation of all the actuators defined as $\hat{F} = [\hat{F}_1, \dots, \hat{F}_m]$ with $\hat{F}_j \in \mathbb{R}^{3 \times 1}$:

$$\hat{F}_j = \frac{F_j}{\|F_j\|}, \quad j = 1, \dots, m. \quad (22)$$

The following Proposition gives sufficient conditions on $s(\tau_d)$ to build such a smoothing

Proposition 1 - Let us consider ∇ the Clarke generalized gradient operator as defined in [22] and the function $s(\tau_d) \in \text{Ker}\{M\}$, $\forall \tau_d \in \mathbb{R}^6$ be such that:

- **C1.** Its gradient is bounded for any bounded τ_d , i.e., there exists $\varepsilon_1(\tau_d) > 0$ such that:

$$\|\nabla s_j(\tau_d)\| \leq \varepsilon_1(\|\tau_d\|), \quad \forall j = 1, \dots, m.$$

- **C2.** There exists a scalar $\varepsilon_2 > 0$ such that for any $\tau_d \in \mathbb{R}^6$:

$$\|F_j^* + s_j(\tau_d)\| \geq \varepsilon_2, \quad \forall j = 1, \dots, m.$$

then the mapping (21) is a solution of the CAP problem that ensures Lipschitz continuity of \hat{F}_j , $j = 1, \dots, m$ on any compact domain $\mathcal{T}_d \subset \mathbb{R}^6$. Moreover, for any compact set \mathcal{T}_d , an upperbound of the Lipschitz constants for each actuator orientation is

$$L^j \leq \frac{2}{\varepsilon_2} \left(\|M_j^\dagger\| + \varepsilon_1 \right), \quad j = 1, \dots, m, \quad (23)$$

where $\varepsilon_1 = \max_{\tau_d \in \mathcal{T}_d} \varepsilon(\tau_d)$, $M_j^\dagger \in \mathbb{R}^{3 \times 6}$ is the sub-matrix of $M^\dagger = [M_1^\dagger, \dots, M_m^\dagger]^T$ associated with the j^{th} actuator.

Proof - To prove the statement, it is enough to show that the jacobian of \hat{F}_j is bounded. Using the formula of derivative of a normalized function from [23] and [24], the jacobian of \hat{F}_j is

$$\nabla \hat{F}_j = \nabla \left(\frac{F_j}{\|F_j\|} \right) \quad (24)$$

$$= \frac{1}{\|F_j\|} \left(I_{3 \times 3} - \frac{F_j F_j^T}{F_j^T F_j} \right) \nabla F_j \quad (25)$$

The norm of (25) can be upperbounded as \hat{F}_j

$$\|\nabla \hat{F}_j\| \leq \frac{1}{\varepsilon_2} \left(1 + \left\| \frac{F_j F_j^T}{F_j^T F_j} \right\| \right) \|\nabla F_j\|. \quad (26)$$

The proof is completed by noticing that for any $\tau_d \in \mathcal{T}_d$:

- $\left\| \frac{F_j F_j^T}{F_j^T F_j} \right\| = 1$;
- $\|\nabla(F_j^* + s_j(\tau_d))\| = \|M_j^\dagger + \nabla s_j\| \leq \|M_j^\dagger\| + \varepsilon_1$

which finally implies :

$$\|\nabla \hat{F}_j\| \leq \frac{2}{\varepsilon_2} (\|M_j^\dagger\| + \varepsilon_1). \quad (27)$$

□

Several ways to build smoothing mapping $s(\tau_d)$ exist. The following proposition gives a systematic way to build a simple smoothing function

Proposition 2 - Let a vector $K_b = [K_{b_1}^T, \dots, K_{b_m}^T]^T \in \text{Ker}\{M\}$ exists such that $\|K_{b_i}\| \geq 1, i = 1, \dots, m$. Let also $K_i \in \mathbb{R}^{3 \times 3}$ be an orthonormal basis such that the first vector of the basis is $K_{b_i}/\|K_{b_i}\|$. Then the smoothing mapping

$$s(\tau_d) = K_b b(\tau_d) \quad (28)$$

satisfies the conditions of Proposition 1 for any scalar positive function $b(\cdot) : \mathbb{R}^6 \rightarrow \mathbb{R}_0^+$ which satisfies the following two equations

$$\|\nabla b(\tau_d)\| \leq \frac{\varepsilon_1(\tau_d)}{\|K_b\|} \quad (29)$$

$$b(\tau_d) \geq \max_{i=1, \dots, m} \frac{\varepsilon_2 - e_1^T K_i^{-1} F_i^*}{\|K_{b_i}\|},$$

if $\min_{i=1, \dots, m} \left\| \begin{bmatrix} e_2^T \\ e_3^T \end{bmatrix} K_i^{-1} F_i^* \right\| < \varepsilon_2$, (30)

where e_i is the i th vector of the canonical basis.

Proof - Condition C1 from Proposition 1 simply follows by substitution.

Condition C2 from Proposition 1 is fulfilled by equation (30). A smoothing action will appear along the nullspace direction K_{b_i} of the i^{th} actuator that produces orthogonally to this direction, a force that falls below ε_2 . This is done by analysing the result $\left\| \begin{bmatrix} e_2^T \\ e_3^T \end{bmatrix} K_i^{-1} F_i^* \right\| < \varepsilon_2$. This enables to counteract all sources of discontinuities in the actuators orientation since the action along the nullspace will ensure in a systematic manner the profile of F . Away from the singularities, the solution F is mainly based of F^* , the Moore-Pseudo inverse solution. Close to the singularities, the action along the null-space becomes proeminent such that a continuous θ orientation is produced. Therefore, any function $b(\tau_d)$ defined as (29)-(30) ensures $\|F_j^* + s_j(\tau_d)\| \geq \varepsilon_2; \forall j = 1, \dots, m$ □

Remark 3 - Although not needed for Proposition 2, in practice it is convenient to add a third condition to $b(\tau_d)$ that is

$$b(\tau_d) = 0, \text{ if } \min_{i=1, \dots, m} \left\| \begin{bmatrix} e_2^T \\ e_3^T \end{bmatrix} K_i^{-1} F_i^* \right\| >> \varepsilon_2. \quad (31)$$

which ensures that under the condition that all actuators have components orthogonal to K_b that are sufficiently large, the mapping (21) coincide with F^* □

Remark 4 - The vector K_b can be interpreted as a "rest configurations" of the actuators which produces zero total force/torque but where all the actuators are producing some thrust. Following the observation of Remark 3, if multiple choices are possible, it is convenient to select K_b in such a way that is orthogonal to the "typical" optimal configurations of the actuators. A possible way to compute K_b is by solving the following optimization problem.

$$\begin{aligned} \min_{K_b} \quad & \|K_b\|_2^2 \\ \text{s.t.} \quad & K_b \in \text{Ker}(M) \\ & \|K_{b_i}\| \geq 1, i = 1, \dots, m \\ & K_{b_i}^T F_i^*(\tau^j) = 0, j = 1, \dots, n_{typical} \end{aligned} \quad (32)$$

where $\tau^j, j = 1, \dots, n_{typical}$ are the "typical" configurations of large forces requested by the vehicle (e.g. forward force in x for a ship, vertical thrust in z for a multirotor, etc). Note that depending the number of actuators and the number of "typical" configurations selected, the problem may become infeasible as it reduces the search space, thus the number of these "typical" configurations must be chosen appropriately. Although (32) is not convex, the problem is still reasonably solvable offline. \square

Remark 5 - An example of function $b(\tau_d)$ which satisfies Proposition 2 is

$$b(\tau_d) = \max \{0, F_{ker_i}\} g(\tau_d) \quad \forall i = 1 \dots m \quad (33)$$

where F_{ker_i} , the force in kernel direction for the i^{th} actuator, is defined as

$$F_{ker_i} = \frac{\varepsilon_2 - e_1^T K_i^{-1} F_i^*}{\|K_{b_i}\|} \quad \forall i = 1 \dots m \quad (34)$$

and $g(\tau_d) : \mathbb{R}^6 \rightarrow \mathbb{R}_0^+$ is a sigmoid-like function such as :

$$g(\tau_d) = -k_a \left(\frac{2}{\pi} \text{atan} \left(k_b \min_{i=1, \dots, m} \left(\left\| \begin{bmatrix} e_2^T \\ e_3^T \end{bmatrix} K_i^{-1} F_i^* \right\| \right) - \varepsilon_1 \right) + 1 \right) \quad (35)$$

with $k_a, k_b \in \mathbb{R}_0^+$ as tuning parameters allowing to choose the ε_1 value and ε_2 the smoothing threshold. In these notations, atan is the arctangent function.

4 Dynamic optimization for constrained control allocation

In many real applications, further constraints in addition to the positivity of the thrust might be imposed such as, e.g. thrust saturations, limited servo velocities, pointing constraints, etc. In these cases, analytical solutions cannot be easily computed and online optimization must be used ([7, 18, 19, 12, 20]). The typical approach presented in the literature to solve this problem while avoiding singularities in the mapping is to consider the problem in discrete time and to solve at each sampling time an optimization problem of the form:

$$\min_{\theta, T, s} \mathbf{J} = T^T W T + s^T Q s + \frac{\varrho}{\epsilon + \det(J(\theta) J^T(\theta))} \quad (36)$$

$$\text{s.t.} \quad \tau_d = J(\theta) T + s \quad (37)$$

where the cost function consists on :

1. $T^T W T$: a quadratic term representing the power consumption of the n actuators;
2. $s^T Q s$: a quadratic term that allows to play on the magnitude of the slack and thus how close to τ_d the produced torques/forces will be ;
3. $\frac{\varrho}{\epsilon + \det(J(\theta) J^T(\theta))}$: a nonlinear term which penalizes coming close to the singularities of $J(\theta)$;

Such a problem can be enhanced with various constraints depending on the type and performances of the actuators such as thrust rate, thrust saturations, angle rate and forbidden constraints.

A major problem of this constrained optimization problem is its non-convexity due to the equality constraint in (37) and the penalty in (36). The penalty $\frac{\varrho}{\epsilon + \det(J(\theta) J^T(\theta))}$ was introduced in [7], based on the fact that $\det(J(\theta) J^T(\theta))$ comes close to 0 near the so-called rank-deficient singularities. This method is still largely used in the marine literature ([25]). The main issues with this approach is that (i) it does not work for all configurations with less vectorized thrusters than

DOFs ($\forall n > m : \det(J(\theta)J^T(\theta)) = 0$) and (ii) it does not provide a systematic solution everywhere, especially around $\tau_d = 0$. While nonlinear problems can be solved by using sequential programming by the means of local approximations at each time instant ([7]-[26]) and/or by considering small variations of the thrusts and angles ([10]), issues (i)-(ii) are usually solved by ad-hoc methods. This section describes how the closed-form continuous solution presented at the previous section can be exploited also to build a smoothing cost function to be used in optimization-based CAP solutions.

The solution proposed in this section is based on the optimization formulation proposed in [8] where the problem (36)-(37) is rewritten using the formalism (12) instead of (10). The main idea of our approach is to add the term $q_1 b(\tau_d) \|K_b^T F - q_2\|_2^2$ in the cost function: when needed, this induces an action in the directions contained in K_b , which is enough to avoid singular configurations and large variations of the thrusters' orientations. The resulting optimization problem is :

$$\min_{F, s, \lambda} \quad F^T W F + s^T Q s + q_1 b(\tau_d) \|K^T F - q_2\|_2^2 \quad (38)$$

$$\text{s.t. } \tau_d = M F + s \quad (39)$$

where $F^T W F$ represents the energy of the actuation and $s^T Q s$ is a slack penalty.

The main advantage of this formulation is that it results in a convex optimization problem. Interestingly enough, various types of typical constraints can be added to this formulation preserving convexity included:

- Saturation constraints on thrust, $\|F_i\| \leq T_{i,max}$;
- Pointing constraints and angular rate constraints by defining suitable convex cones C_i and adding constraints in the form $F_i \in C_i$;

5 Numerical examples

5.1 Application of the Lipschitz continuous control allocation

5.1.1 A 3DOF surface vessel with 3 azimuth thrusters

We consider a supply vessel in 2D with $n = 3$ DOF with a length of 76.2 m and a beam of 19.6 m from [27]. Its body frame \mathbf{B} is the one attached to the coordinate origin of the vessel [28]. The vessel is equipped with $m = 3$ azimuth thrusters located at positions $p_{A_i}^B = [-30, -8, 5]^T, [-30, 8, 5]^T$ and $[30, 0, 5]^T$ m as depicted in figure 4. Considering a fixed elevation angle of $\frac{\pi}{2}$ rad, varying the azimuth angle allows to project the thrust T_i along the x and y axes into a surge force $F_{x_i} = T_i \cos(\beta_i)$ and sway force $F_{y_i} = T_i \sin(\beta_i)$. One can rewrite the force vector as $F = [F_{x_i} F_{y_i}]^T$ and fall back in the formalism of equation (12).

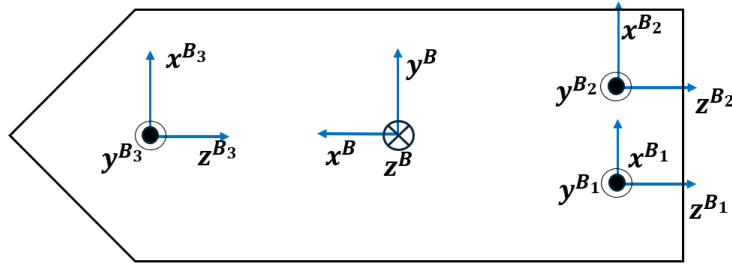


Figure 2: Surface vessel with 3 azimuth thrusters - Body fixed frame \mathbf{B} and the actuator-located \mathbf{B}_i frames.

For this example, let us consider a docking context where the position controller of the vessel is requesting the actuators to produce only forces in surge F_x ranging from - 100 kN to 100 kN such that the vessel goes straight then backwards while keeping the same yaw orientation. F_y and τ_z are then kept zero throughout the whole operation. By following equations (5)-(18), with $P = [e_1 \ e_2 \ e_6]$ and neglecting κ_{d_i} following [28], the mapping matrix $M \in \mathbb{R}^{3 \times 6}$ of equation (12) can be written as :

$$M = \begin{bmatrix} 1 & 0 & 1 & 0 & 1 & 0 \\ 0 & 1 & 0 & 1 & 0 & 1 \\ -l_{y_1} & l_{x_1} & -l_{y_2} & l_{x_2} & -l_{y_3} & l_{x_3} \end{bmatrix} \quad (40)$$

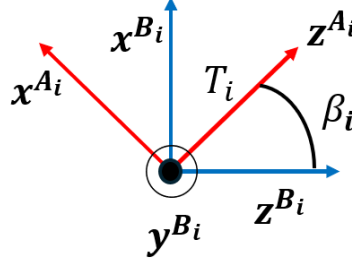


Figure 3: Surface vessel with 3 azimuth thrusters - The actuator-fixed frames A_i associated to the azimuth angles β_i produced by a rotation along the actuator-located y^{B_i} axis. The thrust is produced along the actuator-fixed axis z^{A_i} . The rotation produced a force in the x and y body-framed axes.

where l_{y_i} and l_{x_i} are the $x - y$ coordinates of the position vector $p_{A_i}^B$ of the i^{th} actuator. Being a constant matrix, one can compute offline once and for all its pseudo-inverse $M^\dagger \in \mathbb{R}^{6 \times 3}$, its associated nullspace of dimension 3 in this case and from it, the best smoothing directions $K_b \in \mathbb{R}^{6 \times 1}$ by solving (32). For the current example depicted at Figure 4, $K_b = [0.8517, 0.5241, -0.9731, -0.2290, 0.7071, -0.7071]^T$. With the smoothing function $b(\tau_d)$ defined in (35) with tuning parameters $k_a = 1$, $k_b = 0.1$ and $\varepsilon_2 = 50$, we obtain the results of Figure 4. One can clearly observe the

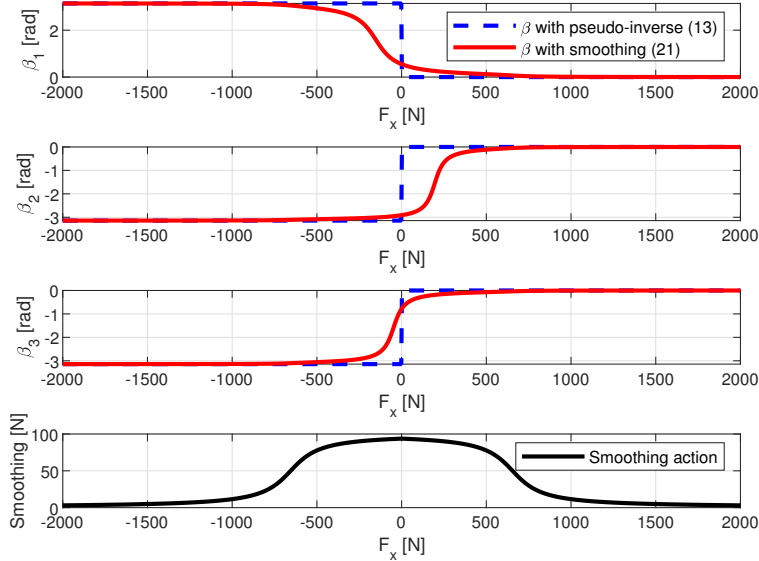


Figure 4: Evolution of the azimuth angles β_i in the neighbourhood of $\tau_d = 0$. Dashed curves are azimuth angles with solution (13), solid curves are the ones with solution (21). The solid black curve is the value of the thrust added in the nullspace direction to perform the smoothing

smoothing action when coming close the discontinuity in $F_x = 0$, $\tau_d = [0, 0, 0]^T$ where with solution (13) a jump from $\pm \pi$ rad to 0 would have occurred. With the action along the null space, each actuator somehow anticipate the change of orientation. This can be tuned by increasing the ε_2 factor which acts like a smoothing threshold. By (30), the bigger ε_2 , the sooner the nullspace action occurs, the less optimal the solution F is since F becomes greater in 2-norm than F^* . This solution can also be used in situation where actuators constraints are not prominent. To conclude, using (27) and computing beforehand the maximum ε_1 over the compact set \mathcal{T}_d , we can compute an upperbound to the Lipschitz constants of $5.68 \frac{\text{rad}}{N}$. We observe within the example a rate of change of the actuator reference of $0.01 \frac{\text{rad}}{N}$. Such a difference can be explained by the size of \mathcal{T}_d : following the condition C1 of Proposition 1 and equation (27), the bigger the considered \mathcal{T}_d , the higher the upperbound can be.

5.1.2 A 6DOF quadcopter UAV with tilting rotors

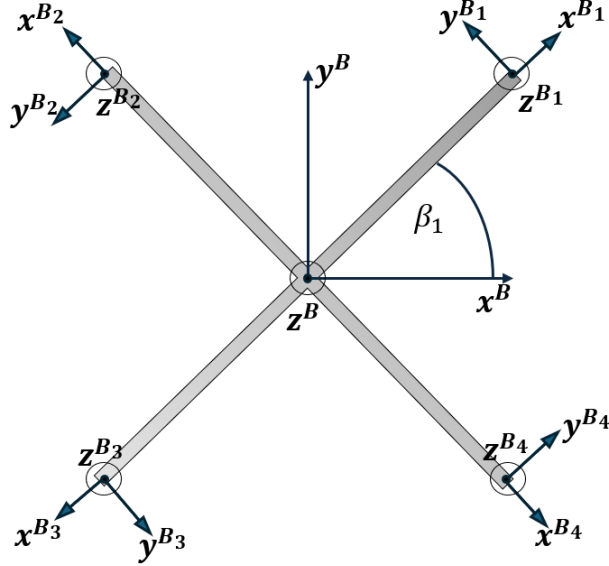


Figure 5: Representation of a X-shaped quadcopter with tilting rotors

For this example, we consider an X-shape quadcopter as depicted on Figure 5 with tilting propellers-rotors units actuated by servomotors as depicted on Figure 6. These allows to produced an thrust T_i in a direction $\theta_i = [\alpha_i, \beta_i]$ for each of the i^{th} unit. Each i^{th} rotor is located at position $p_{A_i}^B = [l_{x_i}, l_{y_i}, l_{z_i}]^T$. The body frame B is attached at the center of the X arms, the frame B_i is located at $p_{A_i}^B$ with an fixed azimuth angle β_i and the frame A_i is an actuator-fixed frame oriented by a varying elevation angle α_i as represented on Figure 5 and 6. The actuators are located at $[1, 0, 0.1]^T$, $[0, 1, 0.1]^T$, $[-1, 0, 0.1]^T$ and $[0, -1, 0.1]^T$ m with an fixed angle vector $\beta = [\pi/4, 3\pi/4, 5\pi/4, 7\pi/4]^T$ rad. In the case

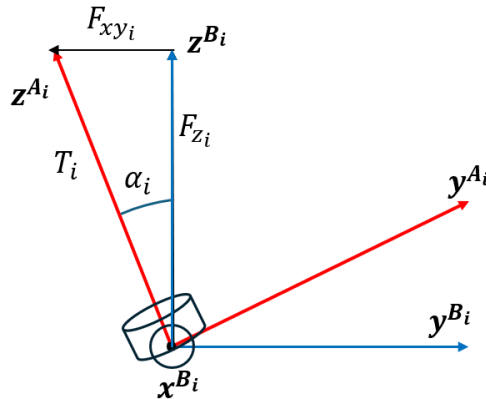


Figure 6: Representation of the actuator-fixed frame A_i and the actuator-located frame B_i - Projection of the thrust T_i on the XY plane and Z direction by a variation of the elevation angle α_i to generate the projected forces F_{xy_i} and F_{z_i}

of an fully-actuated aerial quadcopter, discontinuities such as the one showcased at Figure 4 occurs when performing acrobatics such as flipping and others involving abrupt changes of attitude. Following the solution (21), one can come up with a closed-form solution to the allocation problem. Considering equation (2) with the tilting mechanism in Figure 5 that allows to project the thrust and generate a force F_{xy} in the XY plane and F_z in the Z direction, one can express

for the i^{th} actuator the projected forces and their resulting torques as follows :

$$\tau_{di} = \begin{bmatrix} -T_i \sin(\beta_i) \sin(\alpha_i) \\ T_i \cos(\beta_i) \sin(\alpha_i) \\ T_i \cos(\alpha_i) \\ T_i(l_{y_i} \cos(\alpha_i) - l_{z_i} \cos(\beta_i) \sin(\alpha_i) + \kappa_{di} s_i \sin(\beta_i) \sin(\alpha_i)) \\ -T_i(l_{x_i} \cos(\alpha_i) - l_{z_i} \sin(\beta_i) \sin(\alpha_i) - \kappa_{di} s_i \cos(\beta_i) \sin(\alpha_i)) \\ T_i(l_{x_i} \cos(\beta_i) \sin(\alpha_i) + l_{y_i} \sin(\beta_i) \sin(\alpha_i) - \kappa_{di} s_i \cos(\alpha_i)) \end{bmatrix} \quad (41)$$

By following equations (9) and (5), one can come up with the following extended representation $\tau_d = M^*F$, $M^* \in \mathbb{R}^{6 \times 8}$. By computing the null-space directions $K_b = (0.7071)[-1, 1, -1, -1, 1, 1, 1, -1]^T$, one can see that we indeed obtain a 2D plane of solutions constructed by F_{xy} and F_z along which we can smooth along. Finally, with $F = [F_1 \dots F_n]^T$ such that $F_i = [F_{xy_i} \ F_{z_i}]^T$ where $F_{xy_i} = T_i \sin(\alpha_i)$ and $F_{z_i} = T_i \cos(\alpha_i)$, one can write M^* such that $M^* = [M_1^* \dots M_n^*]$ with M_i^* defined as:

$$M_i^* = \begin{bmatrix} \sin(\beta_i) & 0 \\ -\cos(\beta_i) & 0 \\ 0 & 1 \\ l_{z_i} \cos(\beta_i) - \kappa_{di} s_i \sin(\beta_i) & l_{y_i} \\ l_{z_i} \sin(\beta_i) + \kappa_{di} s_i \cos(\beta_i) & -l_{x_i} \\ -l_{x_i} \cos(\beta_i) - l_{y_i} \cos(\beta_i) & -\kappa_{di} s_i \end{bmatrix}. \quad (42)$$

The case considered here to showcase solution (21) is a 360° flip acrobatic for a change of pitch angle. This is achieved by a variation of the pitch torque. The same smoothing function $b(\tau_d)$ as for the USV example is used with the following parameters : $k_a = 0.1$, $k_b = 1$, $\varepsilon_2 = 3$. To observe the effect of our solution, let us analyse the evolution of the elevation angles in function of the requested pitch torque τ_y from -10Nm to 10Nm .

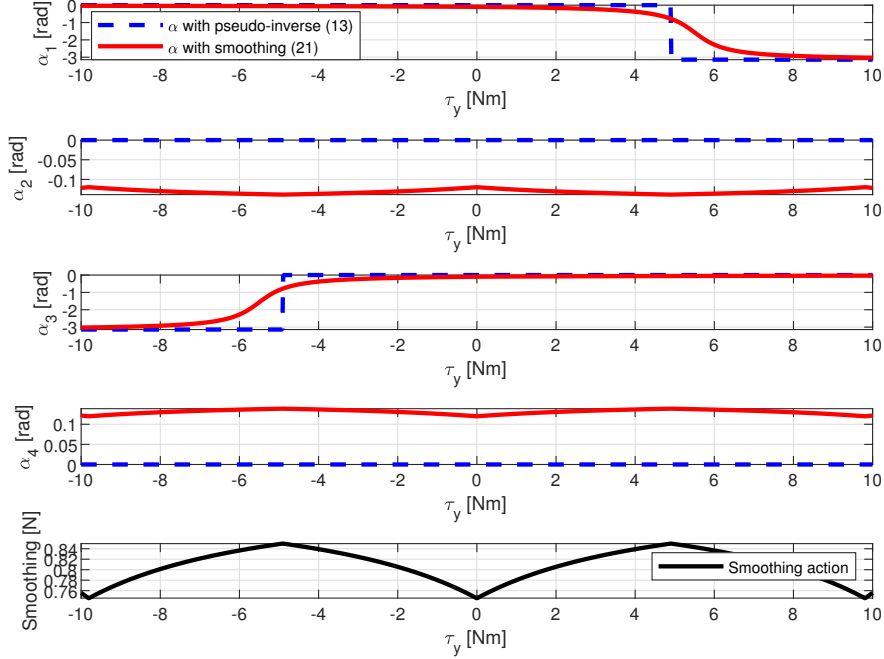


Figure 7: Evolution of the elevation angle references α_i over time. Dashed blue curves are angles without solution (21), solid red curves are with solution (21)

As illustrated in Figure 5.1.2, the application of the smoothing action induces continuous variation in all tilting angles over time. One can see how the smoothing action presents 2 maxima, which occurs whenever one elevation reference presents a discontinuity. The closer to the discontinuity, the bigger the smoothing action becomes. This discontinuity occurs whenever the pilot or the controller would request a pitch torque above half the weight of the UAV, which would require to produce not anymore only a force difference to produce the torque but to exploit the force opposition. This

action along the null space is the key to provide Lipschitz continuity of allocated angles at all times. By computing the upper bound of the Lipschitz constants for the m actuator orientations, we obtain a value of $2.7893 \frac{\text{rad}}{\text{Nm}}$. In the considered example, the observed rate of change of their references is $1.6636 \frac{\text{rad}}{\text{Nm}}$.

5.2 Application of the dynamic optimization for constrained control allocation

In the following section, results of the optimization problem (38)-(39) applied to the 2 case studies are shown. Since by definition, the least expensive solution is the one of the pseudo-inverse, solution (38)-(39) is compared to the solution (13). Furthermore, we will present the results alongside a solution from the literature (equation (36)-(37) from [7]) for the USV case and for the UAV case, we will showcase what would happen if the references based on the pseudo-inverse (13) are directly applied. The optimization problem will consider as constraints the thrust saturation of the actuators T_{max} and the angle rate $\Delta\alpha$ or $\Delta\beta$ to constraint the produced thrust T_i in a cone C_i at each sample time. All the optimization problems in this section and the following are solved using the *MPT3* toolbox ([29]).

5.2.1 A 3DOF surface vessel with 3 azimuth thrusters

In this example, the USV of section 5.1 is considered. The task here is to generate a back and forth manoeuvre in the x -direction. Such an example allows to study the behaviour of the solution around the singularity $\tau_d = 0$. The forces and torques vector τ_d to be produced varies as a sine wave of frequency $f = 0.01$ Hz and of amplitude of $A = 100$ kN for $t = 100$ seconds. We consider as motors parameters : the maximum and minimum azimuth rate of change per second as $\Delta\beta_{max} = 25^\circ$, $\Delta\beta_{min} = -\Delta\beta_{max}$ and the maximum thrust per actuator as $T_{max} = 68$ kN. The elevation α stays fixed at 90° . Tuning parameters for this simulation are : $k_a = 0.008$, $k_b = 0.1$, $\varepsilon_2 = 4500$, $W = 2 \times I_{6x6}$, $Q = W \times 2 \times 10^3$, $q_1 = 0.1$, and $q_2 = 1 \times 10^4$. For solution (36)-(37), tuning parameters are $Q = 2e4 \times I_{3x3}$, $W = 2 \times I_{3x3}$, $\Omega = 1e4 \times I_{3x3}$, $\varrho = 3000$ and $\epsilon = 3e - 10$. For both cases, the initial conditions are the thrusters at rest and pointing stern. Results for solution (38)-(39) are shown alongside those of (36)-(37) and (13).

One can see on Figure 8 that close to $\tau_d = 0$, the action along the nullspace forces the thrusters to rotate early on to reach $\pm\pi$ rad thanks to the penalty introduced in [21]. This allows the thrusters be ready to fulfill the demand of the controller after $t = 50$ s where solution (36)-(37) gets stuck in a local minima and stops producing thrusts as one can see on Figure 9. This deadzone-like effect is dependant on how fast the azimuth reference varies and of course, how fast the servos are. The great advantage of solution (38)-(39) is that it stays as close as possible to the pseudo-inverse one while avoiding to fall in the deadzone caused by the discontinuity of the angle reference. Indeed, one can observe on Figures 9-10 that for $t = [0, 10]$ s and $t = [40, 60]$ s, the smoothing action is more and more predominant which causes a higher thrust and therefore translates into a bigger power consumption of a few %. Away from those time intervals, the solution (38)-(39) performs better than solution (36)-(37). Moreover, this last solution shows hazardous behavior after crossing the $\tau_d = 0$ point at $t = 50$ s as it can be seen on Figure 8 and Figure 10 with random spikes appearing around $t = 55$ s and $t = 91$ s.

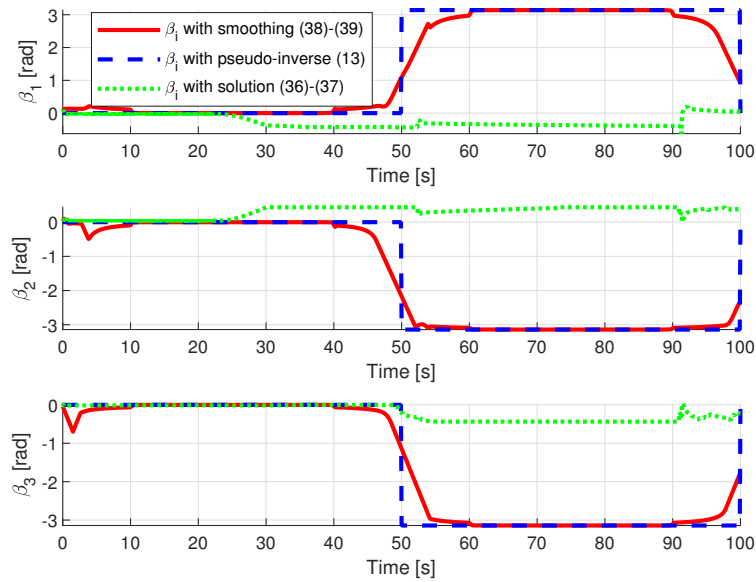


Figure 8: Evolution of the azimuth angles references β_i over time. Green dotted curve is the reference of the angles with solution (36)-(37), blue dashed curve is the reference of the angles with the pseudo-inverse (13) and red solid curve is with the solution (38)-(39)

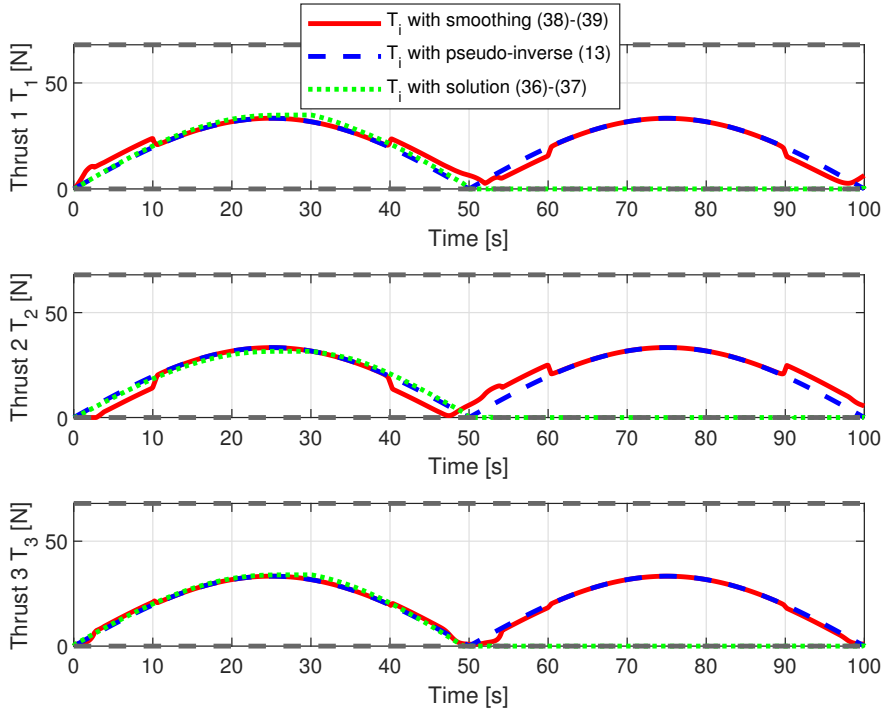


Figure 9: Evolution of the thrusts references T_i over time. Green dotted curve is the thrust reference with solution (36)-(37), blue dashed curve is the thrust reference with pseudo-inverse (13) and red solid curve is with the solution (38)-(39). Black dashed lines are thrust saturation limits.

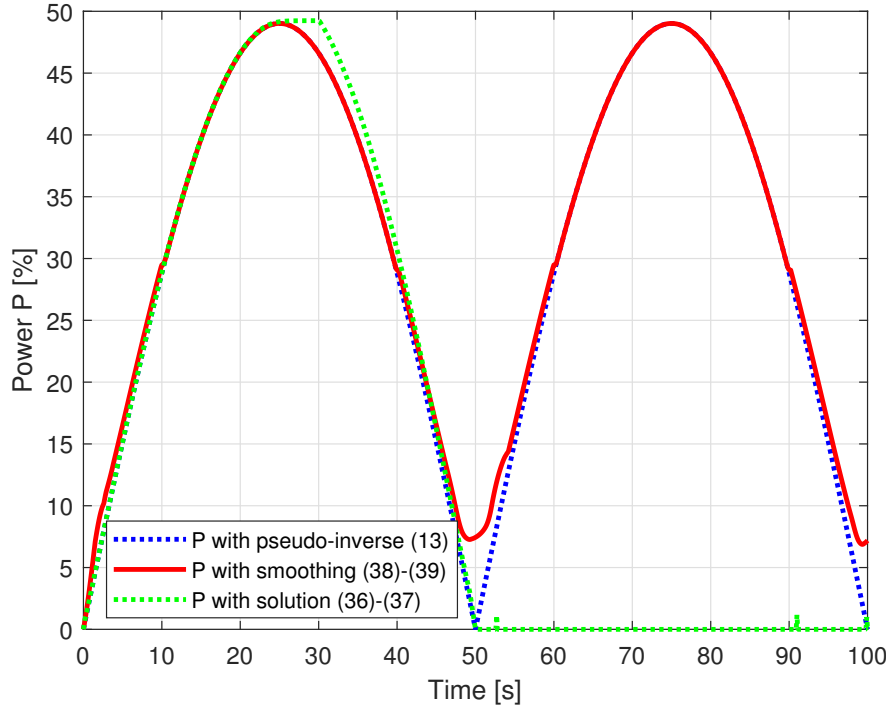


Figure 10: Evolution of the total power consumption of thrusters in % of max power achievable over time. Green dotted curve is the power consumption with solution (36)-(37), blue dashed curve is the power consumption with the pseudo-inverse (13) and red solid curve is with the smoothing (38)-(39)

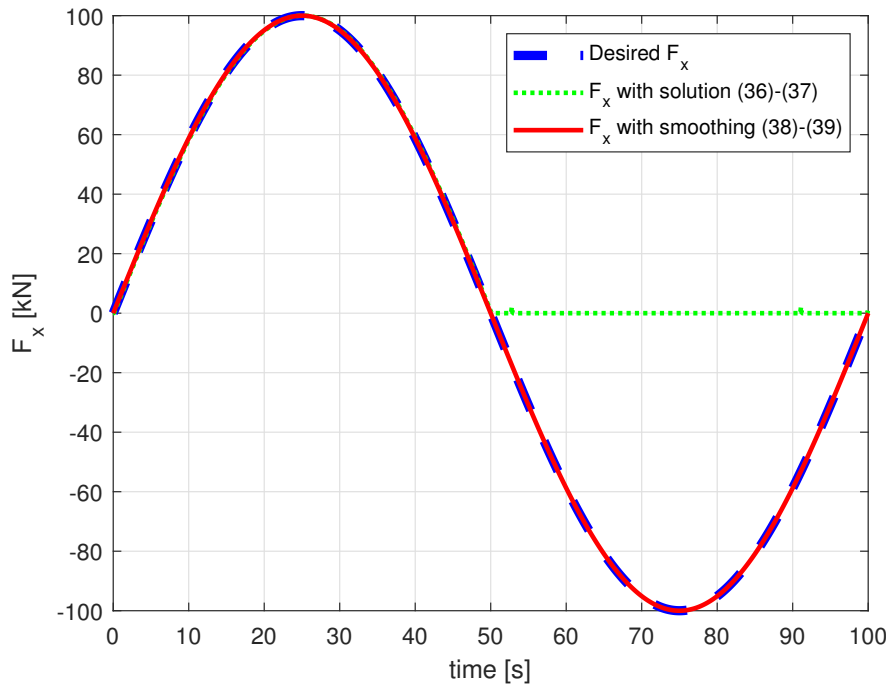


Figure 11: Evolution of F_x over time - Results for a varying surge force as reference. Dashed blue line is the desired F_x obtained from the pseudo-inverse (13), green dotted curve is F_x with solution (36)-(37) and red solid curve is the produced F_x with the smoothing (38)-(39)

5.2.2 A 6DOF quadcopter UAV with tilting rotors

In this case study, we reconsider the quadcopter model from Section 5.1.2 and focus on performing a 360° pitch flip along the y -axis while maintaining gravity compensation. The pilot requests a torque τ_y , which ramps up to 7 Nm within one second before returning to zero. The quadcopter has a mass of 1 kg and is equipped with propeller-rotor (Readytosky 2212 920KV) units that can generate a maximum thrust of 10 N per rotor. The tilting servomotors are assumed to have a maximum rate of 60° per 0.1 seconds. The parameters of the smoothing function $b(\tau_d)$ are kept the same as in Section 5.1.2. The optimization problem is solved using weighting matrices $Q = 2000$, $W = I_{2x2}$, $q_1 = 1$, and $q_2 = 5$. The initial conditions are $\beta = [-0.1047, -0.1047, 0.1047, 0.1047]^T$ rad and the propellers producing only gravity compensation.

Figures 12 and 13 show that our proposed solution, formulated by (38)-(39), is not affected by the discontinuity of angles reference while maintaining continuous thrust and angle references. This ensures that actuator limits are respected within the convex optimization framework. In contrast, when the pseudo-inverse-based method (13) is applied directly, the results show a significant delay in achieving the torque reference, as highlighted in Figures 12-14. However due to the limited angular rate, trying to reach the reference in blue would result in introducing a delay in the loop as one can see it in Figure 14. The discontinuity causes the torque reference to not be reached up to the end of the experiment.

Moreover, Figure 15 illustrates the power consumption during the maneuver. The increased power demand results from the smoothing action applied throughout the flip. The degree of smoothing can be tuned based on specific requirements. A more aggressive smoothing leads to higher power consumption and a less optimal solution, while reduced smoothing achieves a solution closer to the pseudo-inverse one. For high-speed, aggressive maneuvers such as acrobatics, tuning the controller to use minimal smoothing may be advantageous. This ensures rapid responses to sharp variations in the desired α angles, enabling better tracking performance in these scenarios. It is important to note that, as thrust rate dynamics are not taken into account, applying the thrust references from Figure 13 has no observable effect on the power consumption, as demonstrated in Figure 15.

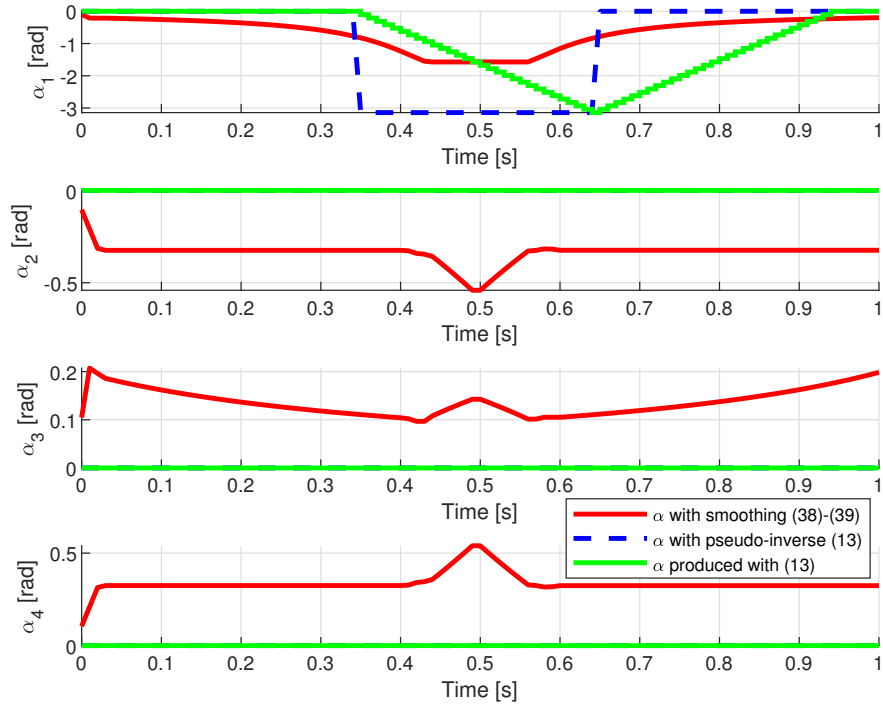


Figure 12: Evolution of the elevation angles reference α_i over time. Blue dashed curve is the reference angles with the pseudo-inverse (13), red solid curve is the allocated angles with the smoothing (38)-(39) and the green solid curve is the result of applying the reference (13) directly to the servos

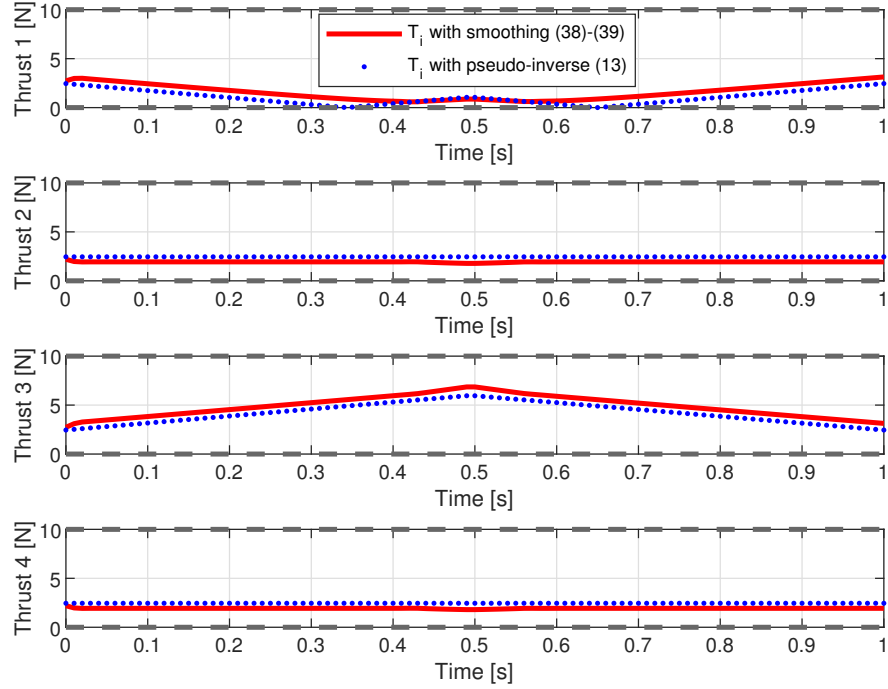


Figure 13: Evolution of the thrusts references T_i over time. Blue dashed curve is the thrust reference with the pseudo-inverse (13) and red solid curve is with the smoothing (38)-(39). Black dashed lines are thrust saturations limits.

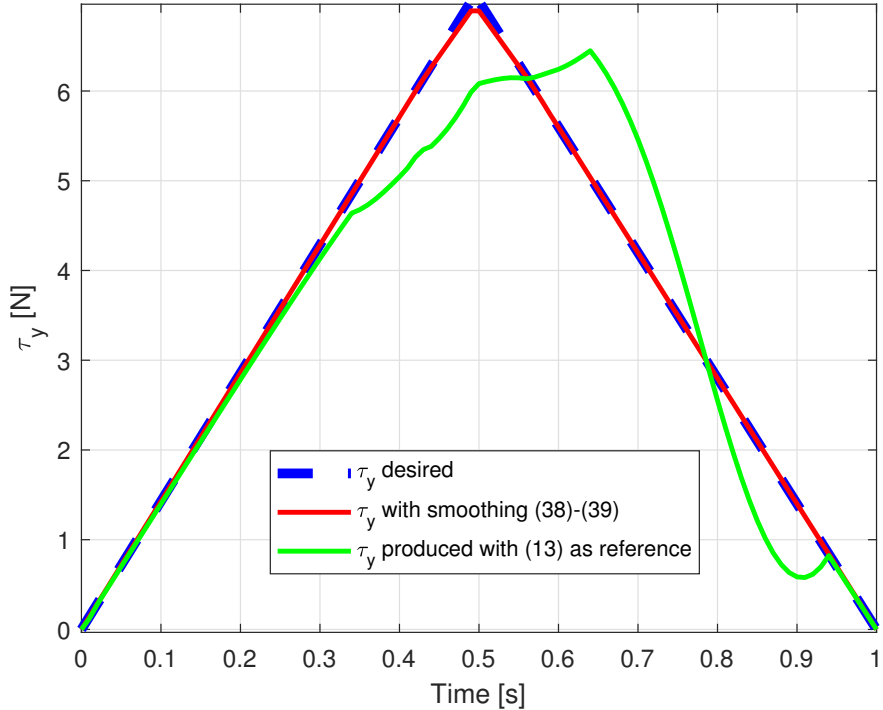


Figure 14: Evolution of the generalized force τ_y over time. Blue dashed curve is the desired torque and red solid curve is the produced torque with the smoothing solution (38)-(39). Green solid curve is the produced torque when the thrust and angle reference of solution (13) are given as thrust and angle reference

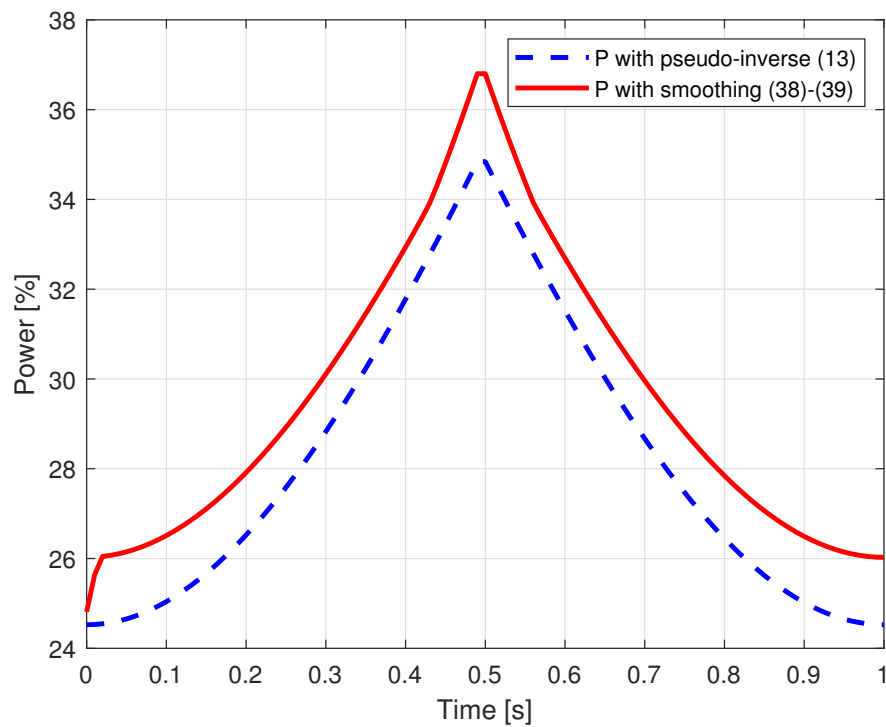


Figure 15: Evolution of the power consumption of thrusters in % of max power achievable over time. Blue dashed curve is with pseudo-inverse (13) and red solid curve is with the smoothing (38)-(39)

6 Conclusion

In this paper, we present two key contributions to the control allocation problem (CAP) for thrust-vector-controlled rigid bodies. The first contribution is a novel closed-form solution that ensures Lipschitz continuity of thruster orientations, addressing all forms of singularities. The second contribution introduces a convex optimization-based formulation of the CAP, which incorporates actuator orientation rate limits and thrust saturation, while assuming negligible thrust rate due to its fast dynamics. This formulation builds on the first contribution, integrating singularity avoidance with a flexible approach that can be extended to accommodate a wide range of actuator constraints.

The effectiveness of both methods has been validated through numerical simulations. Future work will focus on extending these approaches to multi-body systems and scenarios involving varying actuator positions.

References

- [1] Thor I. Fossen and Tor A. Johansen. A Survey of Control Allocation Methods for Ships and Underwater Vehicles. In *2006 14th Mediterranean Conference on Control and Automation*, pages 1–6, June 2006.
- [2] Wayne C. Durham. Constrained control allocation. *Journal of Guidance, Control, and Dynamics*, 16(4):717–725, July 1993. Publisher: American Institute of Aeronautics and Astronautics.
- [3] Kenneth A. Bordingnon and Wayne C. Durham. Closed-form solutions to constrained control allocation problem. *Journal of Guidance, Control, and Dynamics*, 18(5):1000–1007, September 1995. Publisher: American Institute of Aeronautics and Astronautics.
- [4] Kenneth Anthony Bordingnon. *Constrained control allocation for systems with redundant control effectors*. Virginia Polytechnic Institute and State University, 1996.
- [5] Kenneth Bordingnon and Wayne Durham. *Null-space augmented solutions to constrained control allocation problems*. AIAA 1995-3209. Guidance, Navigation, and Control Conference, August 1995.
- [6] T.A. Johansen. Optimizing nonlinear control allocation. In *2004 43rd IEEE Conference on Decision and Control (CDC) (IEEE Cat. No.04CH37601)*, volume 4, pages 3435–3440 Vol.4, 2004.
- [7] Tor Arne Johansen, Thor I Fossen, and Stig P Berge. Constrained nonlinear control allocation with singularity avoidance using sequential quadratic programming. *IEEE Transactions on Control Systems Technology*, 12(1):211–216, 2004.
- [8] Eivind Ruth, Asgeir J Sørensen, and Tristan Perez. Thrust allocation with linear constrained quadratic cost function. *IFAC Proceedings Volumes*, 40(17):337–342, 2007.
- [9] O.J. Sørdalen. Optimal thrust allocation for marine vessels. *Control Engineering Practice*, 5(9):1223–1231, 1997.
- [10] Francesco Scibilia and Roger Skjetne. Constrained Control Allocation for Vessels with Azimuth Thrusters. *IFAC Proceedings Volumes*, 45(27):7–12, January 2012.
- [11] Aleksander Veksler, Tor Arne Johansen, Francesco Borrelli, and Bjørnar Realfsen. Cartesian thrust allocation algorithm with variable direction thrusters, turn rate limits and singularity avoidance. In *2014 IEEE Conference on Control Applications (CCA)*, pages 917–922, 2014.
- [12] Tobias R. Torben, Astrid H. Brodkorb, and Asgeir J. Sørensen. Control Allocation for Double-ended Ferries with Full-scale Experimental Results. *International Journal of Control, Automation and Systems*, 18(3):556–563, March 2020.
- [13] Robert Skulstad, Guoyuan Li, Thor I. Fossen, and Houxiang Zhang. Constrained control allocation for dynamic ship positioning using deep neural network. *Ocean Engineering*, 279:114434, July 2023.
- [14] Huang Huan, Wei Wan, Chunling We, and Yingzi He. Constrained nonlinear control allocation based on deep auto-encoder neural networks. In *2018 European Control Conference (ECC)*, pages 1–8, 2018.
- [15] Mou Chen. Constrained control allocation for overactuated aircraft using a neurodynamic model. *IEEE Transactions on Systems, Man, and Cybernetics: Systems*, 46(12):1630–1641, December 2016.
- [16] Tam W. Nguyen, Kenji Hirata, and Kyoungseok Han. A Nullspace-Based Predictive Control Allocation for the Control of a Quadcopter Manipulating an Object Attached to the Ground. *IFAC-PapersOnLine*, 56(2):6286–6291, January 2023.
- [17] Kongsberg. US type azimuthing thruster - kongsberg maritime. <https://www.kongsberg.com/maritime/products/propulsors-and-propulsion-systems/thrusters/us-azimuthing-thruster/>.

- [18] Xiaocheng Liu, Zhihuan Hu, Ziheng Yang, and Weidong Zhang. Real-time control allocation for autonomous surface vehicle using constrained quadratic programming. *Guidance, Navigation and Control*, 01(04):2140007, 2021.
- [19] Wei Yushi, Mingyu Fu, Jipeng Ning, and Xingyan Sun. Quadratic programming thrust allocation and management for dynamic positioning ships. *TELKOMNIKA Indonesian Journal of Electrical Engineering*, 11, 01 2013.
- [20] Tor A. Johansen, Thor I. Fossen, and Petter Tøndel. Efficient Optimal Constrained Control Allocation via Multiparametric Programming. *Journal of Guidance, Control, and Dynamics*, 28(3):506–515, 2005. Publisher: American Institute of Aeronautics and Astronautics _eprint: <https://doi.org/10.2514/1.10780>.
- [21] Frank Mukwege and Emanuele Garone. On the continuity of control allocation for surface vessels with two azimuth thrusters. *Ocean Engineering*, 287:115813, 2023.
- [22] Frank H. Clarke. *Optimization and Nonsmooth Analysis*. Classics in Applied Mathematics. Springer, New York, 2nd edition edition, 1990.
- [23] Nils Kraemer and M L Braun. Kernelizing pls, degrees of freedom, and efficient model selection. In *Proceedings of the 24th International Conference on Machine Learning*, pages 441–448. Omni Press, 2007.
- [24] Nils Kraemer and Masashi Sugiyama. The degrees of freedom of partial least squares regression. *Journal of the American Statistical Association*, 106(494):697–705, 2011.
- [25] Andreas B. Martinsen, Anastasios M. Lekkas, and Sebastien Gros. Autonomous docking using direct optimal control. *IFAC-PapersOnLine*, 52(21):97–102, January 1 2019.
- [26] Tor A. Johansen and Thor I. Fossen. Control allocation—A survey. *Automatica*, 49(5):1087–1103, May 2013.
- [27] Thor I. Fossen. MSS (Marine Systems Simulator), January 2023. original-date: 2018-10-04T05:12:18Z.
- [28] Thor Fossen. *Handbook of Marine Craft Hydrodynamics and Motion Control*. 05 2011.
- [29] M. Herceg, M. Kvasnica, C.N. Jones, and M. Morari. Multi-Parametric Toolbox 3.0. In *Proc. of the European Control Conference*, pages 502–510, Zürich, Switzerland, July 17–19 2013. <http://control.ee.ethz.ch/~mpt>.